

Lifetime enhancement in the laser-induced periodic surface structures on Si(100) probed by ultrafast transient absorption spectroscopy



Kapil Kumar ^{a,b}, Nikita Vashistha ^{a,b,c}, J.S. Tawale ^{a,b}, Shivam Tiwari ^a, Prince Sharma ^{a,b,d}, Mahesh Kumar ^{a,b,*}

^a CSIR-National Physical Laboratory, Dr. K.S. Krishnan Marg, New Delhi, 110012, India

^b Academy of Scientific and Innovative Research (AcSIR), Ghaziabad, 201002, India

^c Department of Functional Interfaces, Leibniz Institute of Photonic Technology, Albert-Einstein-Straße 9, 07745, Jena, Germany

^d Functional Materials and Microsystems Research Group and the Micro Nano Research Facility, RMIT University, Melbourne, VIC, 3001, Australia

ARTICLE INFO

Keywords:

LIPSS
Laser ablation
Ultrafast transient spectroscopy
Carrier dynamics
Surface states
nanostructuring

ABSTRACT

Laser-induced periodic surface structures are created by irradiating a Si(001) wafer with a femtosecond pulse laser, and then ultrafast transient absorption spectroscopy is carried out on these structures. The ultrafast charge carrier dynamics are reported on the sub-wavelength structuring obtained in a few microns up to hundreds of nm range, which are well below the diffraction limit and reveal the confinement effect. We observed a nearly three-fold increase in the lifetime of the generated hot carriers where several mechanisms and pathways alter the relaxation. The carrier recombination is observed to be slowed down as a result of the confinement due to structuring. This lifetime enhancement is investigated throughout a broad wavelength range of 400–1600 nm. By modulating the periodicity of the surface structures, which is implicitly dependent on the fluence and the number of laser pulses irradiation, it is possible to tune the relaxation lifetime of the material.

1. Introduction

Laser-induced periodic surface structures (LIPSS) can be produced on any material, including metals, semiconductors, and dielectrics [1–5]. Many hypotheses describes the formation of these periodic structures, but no model explains every facet of these periodic patterns. For example, the effect of periodicity on the charge carrier's confinement and photon absorption [6–10]. Until now, the two most prevalent ideas for explaining the development of these structures have been an electromagnetic interaction (scattering and absorption) of microscopic surface roughness and stimulation of surface plasmon polaritons (SPP) and another matter reorganization based on material redistribution near the surface [11–13]. The main difference between the two ideas is that the spatial periodicity is initially seeded along with laser irradiation in the electromagnetic interaction model. In contrast, in matter reorganization, this gets delayed because the material is initially transformed into molten form for a very short duration of laser pulse width and then transforms into ripples due to second pulse irradiation [6]. One theory

based on the instability mechanism also explains the LIPSS formation based on a periodic modulation of the surface temperature irradiating with single femtosecond pulses, which could not explain the inhomogeneous temperature modulation [14]. Sipe's hypothesis is the most widely recognized explanation for the generation of LIPSS [15]. It is based on the electromagnetic interaction of light with surface micro-roughness, which induces a SEW (surface excited wave) similar to SPP's [16]. The periodicity of the structures is determined by material factors such as surface roughness and dielectric permittivity, as well as laser source parameters such as wavelength, polarization, power, pulse duration, repetition rate, and substrate optical properties [3,17–24]. Low spatial frequency LIPSS with periodicity more than half of the incident wavelength ($\lambda > \lambda/2$) and high spatial frequency LIPSS with periodicity less than half of the incident wavelength ($\lambda < \lambda/2$) may be categorized into two groups based on the order of the periodicity [7]. These nanostructures have numerous applications, including absorbing surfaces [25], LIPSS-based waveplates [26], surface color modification [27–29], targeted/selective area patterning like holograms and

Abbreviations: LIPSS, Laser-Induced Periodic Surface Structures; SPP, Surface Plasmon Polaritons; SEW, Surface Excited Wave; UFTS, Ultrafast Transient Absorption Spectroscopy; PIA, Photo-Induced Absorption; SRV, Surface Recombination Velocities; GSB, Ground State Bleach; SRH, Shockley Read Hall; ESA, Excited State Absorption; FFT, Fast Fourier Transform.

* Corresponding author. Academy of Scientific and Innovative Research (AcSIR), Ghaziabad, 201002, India.

E-mail address: mkumar.npl@nic.in (M. Kumar).

<https://doi.org/10.1016/j.physb.2023.414814>

Received 27 December 2022; Received in revised form 26 February 2023; Accepted 12 March 2023

Available online 16 March 2023

0921-4526/© 2023 Elsevier B.V. All rights reserved.

nano-gratings [30], periodic surface defects based on laser-induced alloying [31], plasmonic enhanced devices [32], direct femtosecond laser writing [33–36], fast expanding metamaterials, super wettability [37], bio-medical sensors [38,39], and nonlinear phenomena in materials due to highly spatially selective structuring.

As the phenomenon occurs in a brief period (few ps to ns), its genesis can only be studied using time-resolved spectroscopy with a time resolution better than the formation time. Furthermore, the time-resolved spectroscopy can simultaneously reveal the charge carrier dynamics and be compared to the planar surfaces. Ultrafast transient absorption spectroscopy (UFTS) provides detailed information on the carrier excitation and relaxation in the 10^{-14} to 10^{-9} s (fs-ns) for ultrafast characteristics of a semiconductor device in various optoelectronic capabilities. Si is a well-studied material, and transient absorption spectroscopy has been used in several publications to uncover a variety of phenomena, including band filling, band gap renormalization, photo-induced absorption (PIA), free carrier's densities and lattice heating attributed to electron-phonon coupling [40–42]. It has been observed that the thermalization of hot carriers in crystalline Si occurs across ps timescales, along with different energy transfers in Si reported, such as the transfer of energy from excited carrier to acoustic phonon (0.3 ps), from excited charge carriers to optical phonon (1 ps), and from optical to acoustic phonon (100 ps), respectively [43]. Despite this fact, reports of longer time scale (ns) phenomena, such as recombination in bulk and through the surface states, are also available [44,45]. Surface recombination velocities (SRV) linked to SRH recombination through surface defect state density primarily influences Si wafer carrier lifetime. The quality of a Si wafer is characterized by its lifetime, which means how long the carriers generated can persist before they recombine. These trap states and surface states are the driving factors for the lifetime of the wafer. The photoexcited carriers can recombine in bulk by the radiative band-to-band transition or non-radiative auger and SRH recombination through trapping centers and also recombine on the surface through surface defect states; their combined effect gives us an effective lifetime mentioned in equations (1) and (2) [46]. These trapping centers are due to crystallographic defects and concentration of doping level, while the surface defect states are due to dangling bonds present at the surface and interrupted crystal lattice at the surface [47]. Surface photovoltaics (SPV) spectroscopy has been intensively used to study the surface states of porous and nanostructured Si [48,49]. Nowadays, ultrafast transient absorption spectroscopy, ultrafast transient photoemission spectroscopy, and time-resolved THz spectroscopy are essential tools revealing the different photophysical components of the decay mechanism.

$$\frac{1}{\tau_{\text{eff}}} = \frac{1}{\tau_b} + \frac{1}{\tau_s} \quad (1)$$

Where $\tau_s = W/2S$, S is surface recombination velocity, and W is the thickness of the wafer.

$$\frac{1}{\tau_b} = \frac{1}{\tau_{\text{rad}}} + \frac{1}{\tau_{\text{auger}}} + \frac{1}{\tau_{\text{SRH}}} \quad (2)$$

Where τ_{eff} , τ_b , τ_s , τ_{rad} , τ_{auger} , and τ_{SRH} are effective lifetime, bulk lifetime, surface recombination lifetime, radiative lifetime, auger recombination, and Shockley Read Hall recombination lifetime respectively. As Si is an indirect semiconductor, decay is only non-radiative, and recombination is purely through the auger and SRH recombination through intrinsic defects and doping of the material. Surface processing also creates surface defects, such as surface states near the band edge. Sometimes tail states also appear just below the conduction band due to structural disorders and impurities present at the surface [50]. The surface recombination velocity plays a significant role in recombination; SRV values greater than 10^{-4} cm $^{-1}$ show quicker recombination and is insignificant in bulk diffusion, whereas an SRV gradient of 3×10^{-4} cm $^{-1}$ is reported with fast recombination for Si(001) [45]. More surface recombination is stimulated by a significant increased gradient

produced by a higher SRV value, while bulk recombination supersedes for $S < 10^{-4}$ cm $^{-1}$. The primary mechanism regulating surface recombination is SRV picosecond (ps) time dependence, which shows slower decay at a longer time scale. Another impact may be band banding, which drives carriers from the surface states to reduce recombination [45].

In the present study, we have performed UFTS on generated nanostructure (LIPSS), which shows a prominent lifetime enhancement covering a wide range of wavelengths. The lifetime is mainly affected by increased surface states, defect centers, and surface-to-volume aspect ratio owing to laser-induced structuring and trapping of these carriers in these band-gap states during decay, and the enhanced photo-absorption and confinement slow down the carrier recombination in defect states [51]. Prolonged excited-state relaxations are driven by higher defect concentrations and are related to better charge separation. These nanostructures improve carrier trapping and confinement, lowering surface recombination velocity and thereby reducing the probability of recombination [52]. However, while laser irradiation, foreign oxygen atoms incorporated with Si formed a bond at the surface, which creates a defect in the material. Also, a transition of crystalline Si to amorphous Si is observed. While working with Si-based chips and devices, this foreign oxygen influences the efficiency, so removing oxygen post-structuring is necessary [53]. In the present study, fabrication of nano/microstructure is limited to the area of our spot size of laser beam ~ 65 μm at focus and from a few hundred μm to 1–2 mm out focus along the focal plane. Larger area structuring can be done by line-by-line scanning (2-D) with x-y overlapping of successive pulses [54].

2. Experimental procedure

We employ a titanium sapphire-based laser amplifier (coherent) in our experimental setup, which is a linearly polarised pulse laser system with 800 nm central wavelength, a pulse width of 40 fs, a spectral width of 60 nm, and a repetition rate of 1 kHz and the same is used in pump-probe spectroscopic measurement [45]. The experiment is performed on ultrasonically cleaned n-type Si(001) in an ambient air environment with an average energy of 1 mJ at an angle slightly less than normal incidence to minimize back reflection, and the sample is placed on a translational stage which has a step size of 1/60th of mm. To concentrate the beam energy to the desired region, we employed a 10 cm focal length convex mirror.

The sample is scanned along the laser propagation path at various distances from the lens ranging from 5 cm to 10 cm (a focal point of the lens). Peak fluence and spot size are 30 J/cm 2 and 65 μm , respectively, at the focus point, as estimated by the following formulas:

$$\text{Spot size} = (1.27 * \lambda * f) / D, \quad (3)$$

$$\text{Peak fluence} = \text{Average energy} / \text{spot area}$$

Where average energy is calculated by average power divided by repetition rate and f is the focal length of the lens, D (1.5 mm) is $(1/e^2)$ size of the spot initially at lens calculated from laser beam profile as shown in Fig. 1(a).

3. Results and discussion

3.1. Focal position/fluence dependent periodicity and morphology of LIPSS

Many reports explore the fluence dependency of LIPSS development; by altering the number of pulses exposed and fluence, as well as the location of the sample along the focal plane, which can tune the periodicity of these structures [6,17,18,23]. In the current studies, we varied the distance from 5 cm to 10 cm (at focus), which indirectly changed the fluence. At a distance of 5 cm (Distance is being measured from the lens to the focal point), the laser begins etching the material, but no

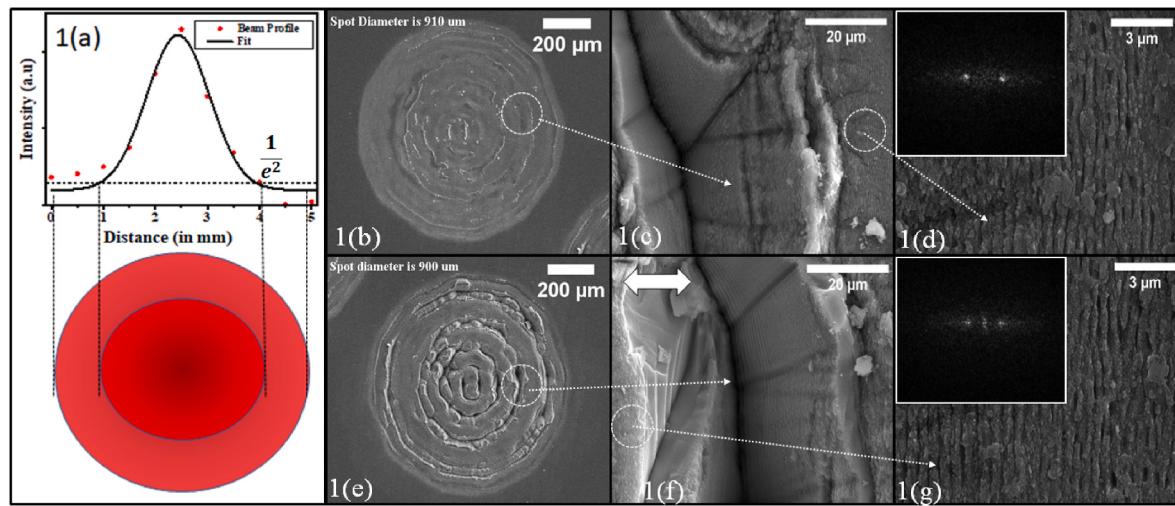


Fig. 1. (a) shows the beam profile of the laser used in the experiment, (b)–(g) SEM image showing surface morphology with 10-sec exposure at two positions, (b) to (d) at 7 cm and (e) to (g) at 8 cm along the focal plane where f (10 cm) is the focal length of the lens and double-sided arrow in 1(f) shows electric field direction.

significant periodic structuring is noticed; when it moves closer to the focus, ablation begins over a greater region, and considerable structuring is observed in areas with higher fluence. We got better outcomes with better ordering with a periodicity of $\sim 0.71\lambda$ and $\sim 0.73\lambda$ at a distance of 7 cm and 8 cm, respectively, from the lens shown in Fig. 1(d and g). Periodic patterns are noticeable in some areas at a distance of 6 cm and 9 cm. For example, it is observable in high fluence areas for 6 cm in central regions, while for 9 cm, it is observable in outer annular rings at a lower fluence region of the laser beam profile. While moving closer to the focus, only the material ablation with no noticeable structures and just the ablation crater is visible in the center, which can be seen in Fig. S1(supporting information). At the same time, the two spots formed at (5 cm and 8 cm) with varied fluences are subjected to ultrafast transient spectroscopy (UFTS).

In Fig. 2, we can see that the circular orientation at different annular regions is due to the gaussian profile of the laser. As the laser system is a femtosecond pulse laser, in 10 s, it produces almost 10 k laser trains, so here we see the combined effect of these multiple pulses; this is the

reason that at many annular regions, valleys formed due to multiple laser trains, also in each annular region periodicity slightly differs from the preceding regions. It can be seen as moving towards the focus, the diameter of the spot is decreased from 1450 nm at 5 cm to 700 nm at the focus where only ablation crater formed at the center and no periodic surface structures is observed. As moving towards the focal point fluence of the laser increases, the transition of nano ripples to micro-spikes and nanoholes is observed. Due to multiple laser pulse irradiation in a single shot, perfect periodic surface structures over the whole irradiated spot area are not observed; mostly, nano ripples with protrusions and nanoholes are observed. The root cause of this transition is the formation of distinct micro ripples in the first few laser pulses; however, after subsequent pulses, owing to modulation ablation, these ripples begin to deform as energy accumulates in holes. With further increase in fluence, these micro protrusions and holes get melted, and micro-spikes formed with orientation as parent ripples, confirming they are transformed in this form from original well-shaped ripples. More increased fluence destroys the symmetry, and clusters of materials along valleys in annular

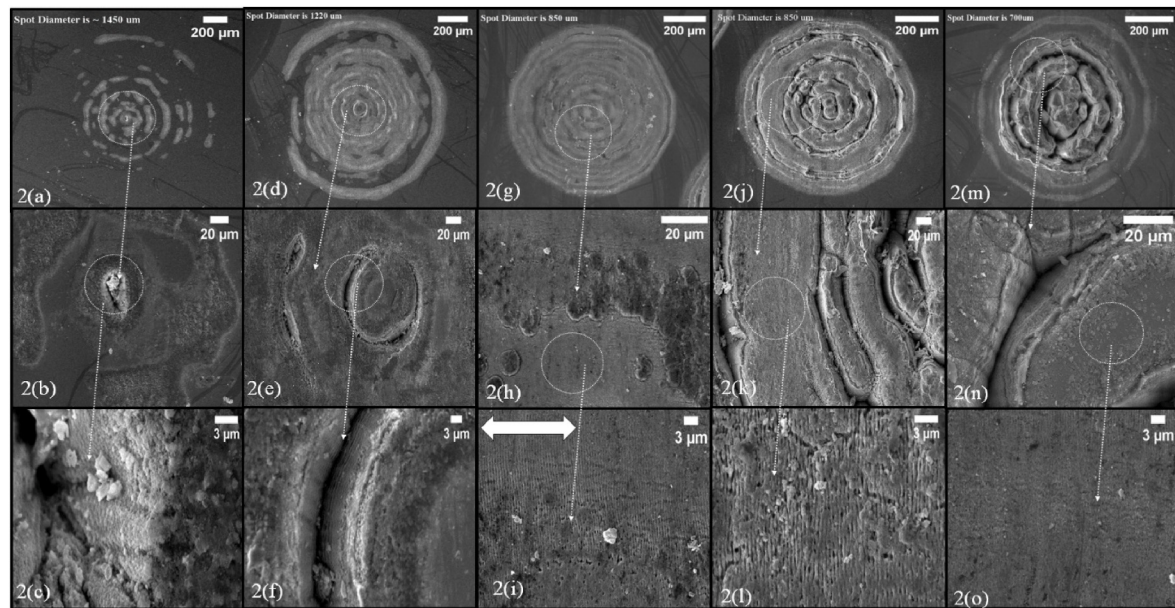


Fig. 2. SEM image of surface morphology (Si coated with 10 nm Gold) with 10-sec exposure positions (a) to (c) at 5 cm, (d) to (f) at 6 cm, (g) to (i) at 7 cm, (j) to (l) at 8 cm and (m) to (o) at 9 cm along the focal plane at different magnifications where Z (10 cm) is focal plane and double-sided Arrow shows electric field direction.

regions are formed. Although near the focus at 9 cm, periodic structures are present, merged with micro clusters, as shown in Fig. 2(o).

3.2. Number of pulses irradiated dependent periodicity and morphology

Furthermore, we have expanded the experiment to investigate how the periodicity and orientation of periodic structures change by altering the laser fluence, i.e., the number of pulses irradiated on the sample. A detailed description is explained below and can be visualized in Figs. 3 and 4. We have done the same set of experiments at a fixed distance (8 cm) from the lens along the focal plane with different exposure duration. By changing the exposure duration, we are changing the number of laser pulses hit in a single shot and finding how the periodicity changes. Figs. 3 and 4 show SEM micrographs for different exposure times. To analyze the SEM images for surface morphological changes, periodicity and profile of the generated periodic structures, an image analysis software SPIP (Scanning Probe Image Processor, SPIP™ Version 4.8) [55,56] is used. Simultaneously 2-D-FFT and 1-D-FFT are performed using SPIP software to determine the periodicity and orientation of the structuring [57], with the varying number of pulses that indicates the number of pulses dependency of LIPSS.

We have analyzed each spot in two different regions, one inner region and another in the outer region (one region at low fluence and the other at high fluence area in accordance to beam profile); in these two regions, we can see the transition of periodicity and orientation of LIPSS with fluence, and also change in periodicity with the varying number of pulses is also observed in each micrograph. The orientation of periodic structures in each of the regions analyzed and determined by 2-D FFT, shown in the inset of the respective SEM micrograph. In Fig. 5 the periodicity given by 1-D FFT of SEM micrograph is shown and mentioned in Table 1. In the outer region of the spot, sharp periodic structures are formed (LSFL), but in the inner region, nano ripples with nano protrusions and nano-holes, which are not so periodic (HSFL), are formed due to high fluence. In both regions at a larger exposure time (30 s), ablation starts in the center, and nano spikes are observed in the inner and outer region of the spot due to multiple pulse irradiation (high fluence), giving multiple times melting of surface materials loses its periodicity. Fig. 4 shows full area scanning of the spot for a 1-sec exposure duration; here figure reveals that there is a transition in

Table 1
Periodicity at different exposure time.

Exposure time (sec.)	Periodicity inner region (nm)	Periodicity in the outer region (nm)
1	230	609
2	370	598
5	429	590
10	280	480
20	321	580

periodicity from the center of the spot to the outer edge of the annular ring. Despite high fluence (Beam profile) in the center of the spot, clear ripples are formed in initial pulse irradiation, but multiple pulses create the nano-holes, and repetitive melting of material creates nano protrusion between two ripples, but in the outer region, clean ripples are observed. As the calculated values in Table 1 which depict that in the central region of the beam profile where the fluence is high, periodic structures formed are High Spatial Frequency LIPSS (HSFL), and at the edges of the beam profile i.e. lower fluence region periodic structures formed are Low Spatial Frequency LIPSS (LSFL). Both types of structures are oriented perpendicular to field polarization.

3.3. Ultrafast Transient absorption spectroscopy on LIPSS

For deeper aspects of the carrier's lifetimes, ultrafast transient absorption spectroscopy (UFTS) [58–61] is performed on the conspicuous spots (generated LIPSS). It compares the lifetime of the planar and the structured surfaces. Differential absorption spectra (ΔA) of planar Si (100) and structured Si (LIPSS at 5 cm) are stimulated with a 410 nm pump wavelength (3.02 eV), and detection is carried out in the wide NIR range of 800–1500 nm (0.82–1.55 eV) shown in Fig. 6 (a) & (b) in their corresponding 2-D color contour plots. In both, structured and planar Si, a significant positive signal PIA (Photo Induced Absorption) is observed, which is attributed to further excitation of excited carriers (excited state absorption-ESA) to higher available states. The signal last for a more extended period for structured Si comparable to planar Si wafer, can be seen clearly in contour plots. For quantitative analysis of lifetime, the multiexponential fitted kinetics ((ΔA) vs. time) in Fig. 7(a) and (b) depicts the decay profile of hot carriers at various wavelengths on a

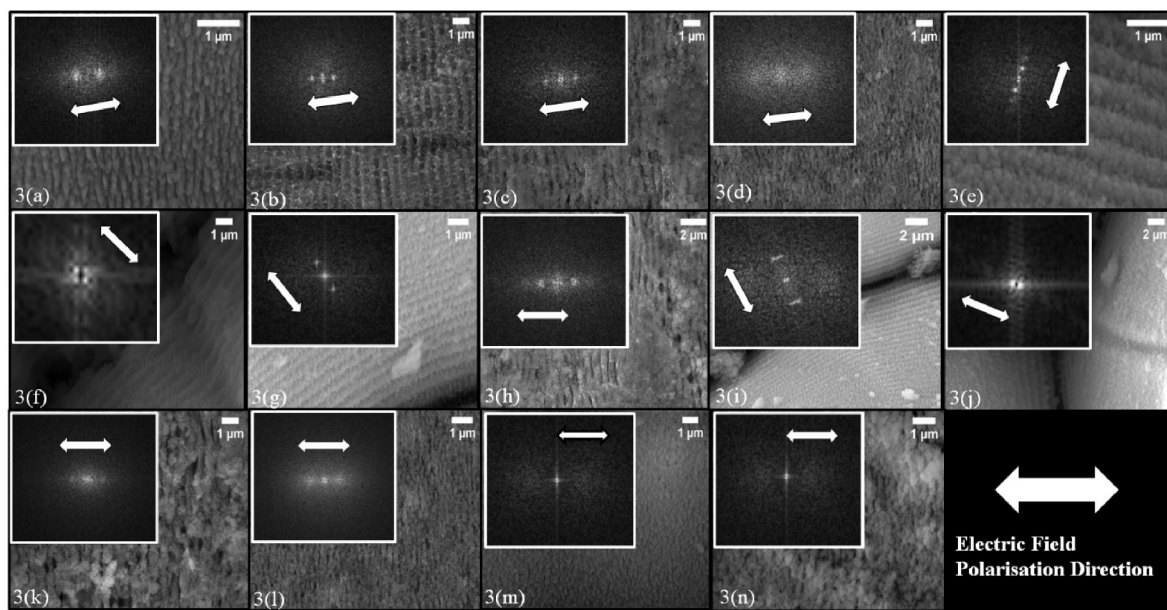


Fig. 3. SEM image of surface morphology at position 8 cm along the focal plane with varying exposure time (a)& (b) for 2 s, (c) to (f) for 5 s, (g) to (i) for 10 s, (j) to (l) for 20 s and (m) &(n) for 30 s along the focal plane at different magnifications where Z = 10 cm is focal plane and white arrow in the bottom right corner shows electric field direction and in the inset of each image represents 2-D FFT and orientation of LIPSS.

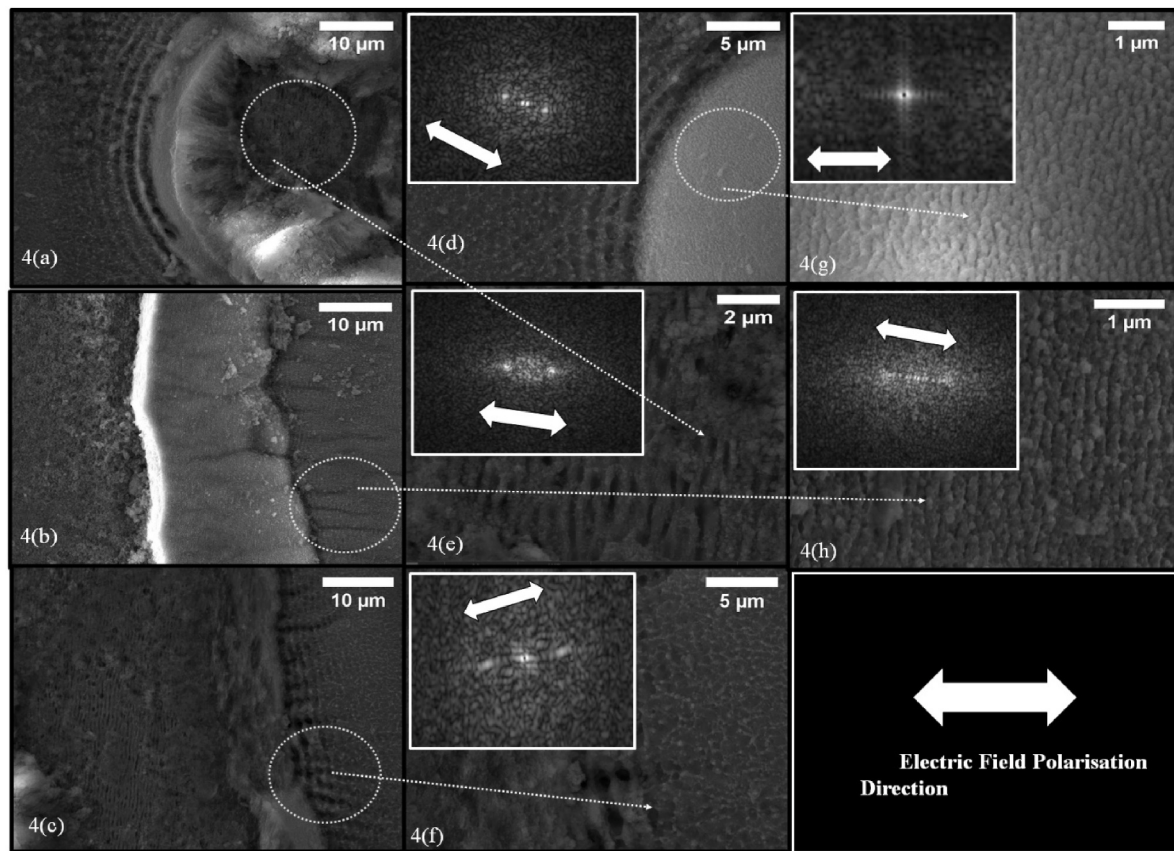


Fig. 4. SEM image of surface morphology at position 8 cm along the focal plane for 1 s exposure time (a), (b) & (c) are the images at different areas of exposure, (d) & (g), (e) & (h), & (f) are higher resolution of (a), (b) & (c) respectively and white arrow in bottom right shows electric field direction and in the inset of each image represents 2-D FFT and orientation of LIPSS.

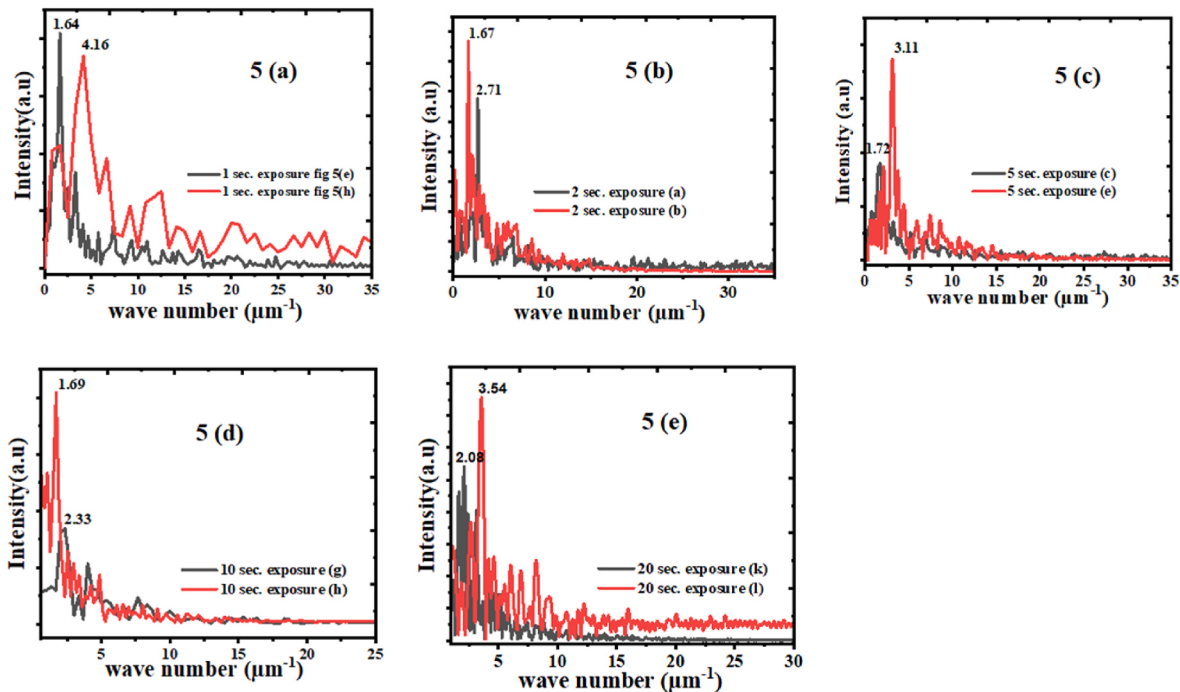


Fig. 5. 1-D FFT of SEM micrographs, (a) to (e) for 1, 2, 5, 10, and 20 s, exposure time, respectively, at a fixed focal position (8 cm).

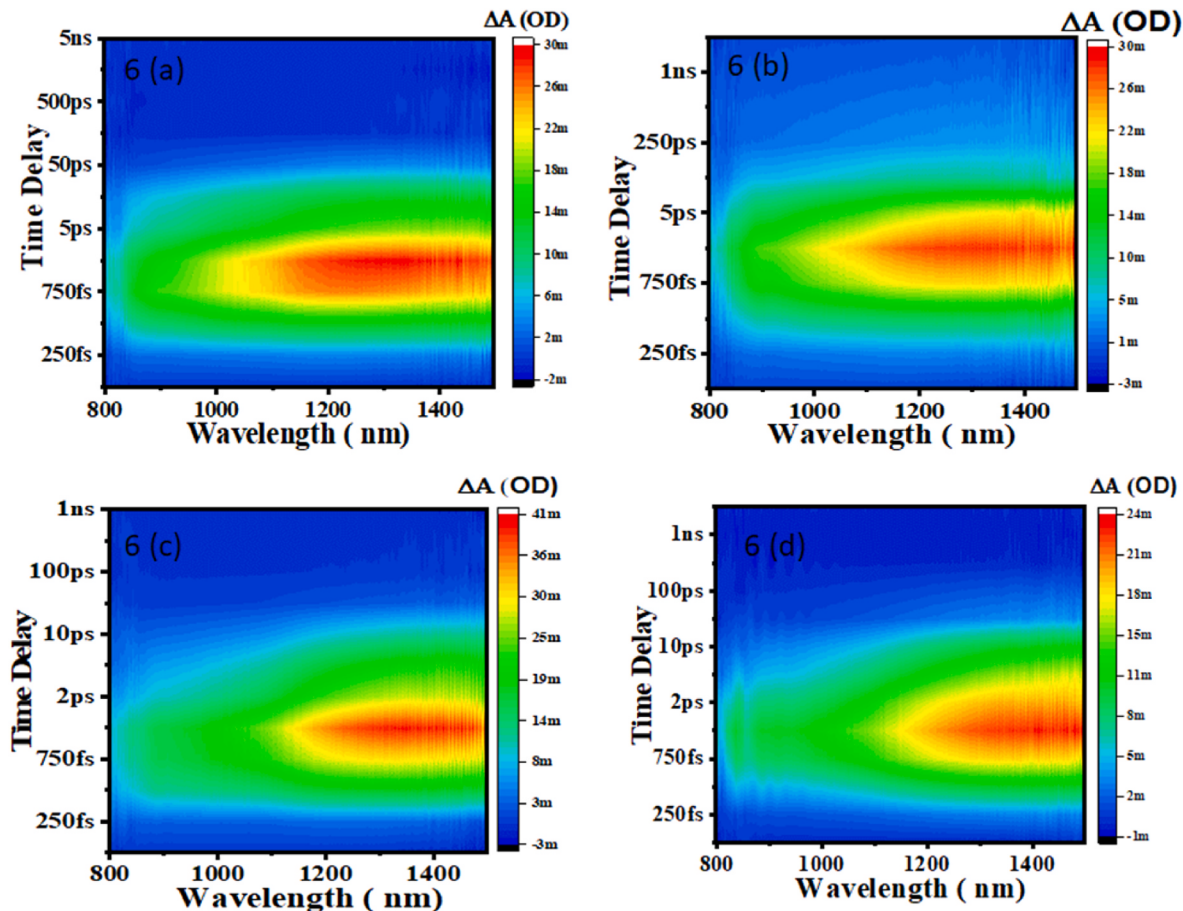


Fig. 6. 2-D color contour plot of transient absorption spectrum (a) planar Si without structuring, (b) Structured Si (LIPSS at 5 cm), (c) Gold coated Planar Si, and (d) Gold coated on structured Si (LIPSS at 5 cm) at different probe wavelength in a wide time window (0–6 ns).

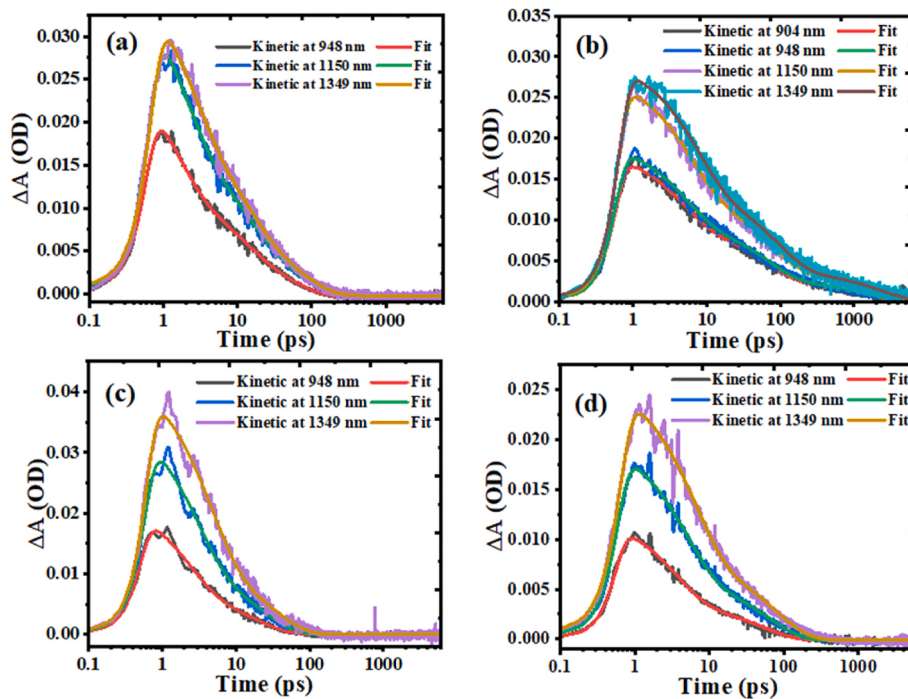


Fig. 7. Kinetic/Decay profile (a) planar Si without structuring, (b) Structured Si (LIPSS at 5 cm), (c) Gold coated Planar Si, and (d) Gold coated on structured Si (LIPSS at 5 cm) at different probe wavelength in a wide time window (0–6 ns), where the X-axis is in log scale.

temporal scale (0–6 ns).

The nano-sized Structuring enhances the light-matter interaction, enhances absorption, and light confinement, which increases the lifetime of the generated hot carrier, is seen throughout the NIR regime of the probe. Differential absorption spectra in both cases show a large positive PIA (Photo Induced Absorption due to probe absorption) signal owing to excited state absorption, which is caused by additional excitation of hot carriers stimulated by the pump to higher excited states shown in respective spectra Fig. S2 (Supporting information). After a few ps, the PIA signal at higher wavelengths increases owing to the re-absorption of thermally relaxed carriers from the band edge of the conduction band and the filled surface states (restricting further carriers to decay). In planar Si, the decay of this signal is substantially faster in the region above the band gap of Si than in the region below the band gap, which is not seen in structured Si, indicating a shift in the band gap. Also, after 5 ps, the signal decay is substantially slower, and this increase in lifetime is observable in structured Si carrier dynamics at various probe wavelengths. The multi-exponential fitting of kinetic profiles reveals the increased relaxation time and pathways followed by hot carriers' decays depicted in Schematic diagram Fig. 9(d). Using the formula below, the kinetic profiles are multiexponential fitted using Surface Xplorer software.

$$C_i^*(t) = IRF \times C_i \quad (4)$$

$$C_i^*(t) = e^{-\left(\frac{t-\tau_0}{\tau_p}\right)^2} \times \sum_i A_i e^{-\left(\frac{t-\tau_i}{\tau_i}\right)} \quad (5)$$

Here, IRF is the instrument response function, C_i undistorted draw kinetic profile, C_i^* is the convolved output, τ_p is FWHM of IRF, τ_0 is time while A_i and τ_i are the i th component amplitude contribution and an i th component of decay time.

Table 2 shows time constants corresponding to decay through carrier-carrier scattering and carrier-phonon relaxation within the conduction band (τ_1), direct relaxation of hot carriers into surface states and intervalley relaxation (τ_2), and direct carrier recombination through tail states of the conduction band results of injected doping level(τ_3). In

Table 2
Decay Kinetics at different probe wavelengths (NIR) for plane and structured Si.

Wavelength (nm)	Plane Si (ps)	LIPSS on Si (5 cm) (%)	Gold on Si (ps)	Gold on LIPSS (5 cm) (ps)	Gold on LIPSS (8 cm) (ps)
948	$\tau_1 = 1.46$ (49%)	$\tau_1 = 4.95$ (67%)	$\tau_1 = 2.24$ (67%)	$\tau_1 = 3.57$ (68%)	$\tau_1 = 2.49$ (64%)
	$\tau_2 = 11.2$ (28%)	$\tau_2 = 67.3$ (38%)	$\tau_2 = 18.8$ (33%)	$\tau_2 = 53.9$ (32%)	$\tau_2 = 40.4$ (36%)
	$\tau_3 = 52.2$ (23%)	$\tau_3 = 1550$ (14%)			
1150	$\tau_1 = 1.93$ (49%)	$\tau_1 = 5.98$ (51%)	$\tau_1 = 2.95$ (69%)	$\tau_1 = 4.83$ (68%)	$\tau_1 = 3.75$ (67%)
	$\tau_2 = 13.6$ (31%)	$\tau_2 = 77.7$ (36%)	$\tau_2 = 23.7$ (31%)	$\tau_2 = 64.8$ (32%)	$\tau_2 = 56$ (33%)
	$\tau_3 = 65.9$ (20%)	$\tau_3 = 1900$ (13%)			
1350	$\tau_1 = 2.46$ (45%)	$\tau_1 = 7.31$ (52%)	$\tau_1 = 4.46$ (73%)	$\tau_1 = 6.3$ (68%)	$\tau_1 = 4.96$ (71%)
	$\tau_2 = 13.6$ (31%)	$\tau_2 = 91.6$ (36%)	$\tau_2 = 33.9$ (27%)	$\tau_2 = 80.7$ (32%)	$\tau_2 = 70$ (29%)
	$\tau_3 = 72.8$ (22%)	$\tau_3 = 2400$ (13%)			

structured Si, a lifetime enhancement of 3-fold in (τ_1) & (τ_2) and multiple-fold enhancement in (τ_3) is observed.

However, the surface recombination velocity rises as the surface area increases, and enhanced recombination velocity tends to result in more recombination; however, this factor is reduced by a SiO_2 passivation layer caused by open-air laser irradiation [62]. These structures improve photon absorption and carrier confinement, increasing hot carrier concentration, restricting carrier concentration movement to the non-radiative recombination centers, and causing an enhancement in carrier lifetime. Since Si is an indirect band gap material, radiative recombination is not detected; instead, the carrier decays through the surface, and SRH recombination is observed due to mostly intrinsic defect states and bulk states. To comprehend sample carrier dynamics, we developed a model to describe the carrier decay process/pathways seen in Fig. 9(d).

The same sample is further coated with a 10 nm thin gold film by RF sputtering, which did not affect the periodicity of these structures can be seen in Fig. 2. UFTS is also performed on the same to study the influence of structuring on the plasmonic behavior and photon confinement due to gold embedded in structured Si (LIPSS) and compared with planar gold film. UFTS is performed with a pump at 410 nm (3.02 eV), much larger than the interband transition threshold (2.38 eV) for both planar gold and gold-embedded structured films (LIPSS at 5 cm), UFTS data shows similar lifetime enhancement as observed for Structured Si. A wide PIA signal is observed over a broad spectrum (475–1500 nm in supporting information Fig. S3) attributed to ESA, which is shown in the 2-D contour plot in Fig. 6(c) & (d) for the NIR regime and Fig. 8(b) and (d) in the visible regime. Furthermore, the multiexponential fitted kinetic profile for carrier decay is shown in Fig. 7(c) and (d), giving the quantitative enhancement in a lifetime. PIA signal is much higher for longer wavelengths (high-intensity data seen in contour plot for longer wavelengths) due to the re-absorption of thermally relaxed carriers from band edge and filled surface states. Two exponential fitting of kinetic profile depicts two-time constant τ_1 corresponds to carrier-carrier relaxation and carrier-phonon relaxation within the conduction band (Intraband-transition) and inter valley relaxation and τ_2 corresponds to phonon-phonon relaxation and transferring the energy to lattice in the form of heat and also to metal-semiconductor interface. Furthermore, the UFTS is also performed on another spot (LIPSS at 8 cm) to confirm similar lifetime enhancement owing to this nano-structuring, the sample is again excited with 410 nm, and detection is done in a wide range Vis-NIR (400–1600 nm). Fig. 9 (a & c) show the kinetic profile of gold-coated LIPSS (8 cm) in NIR (800–1500 nm) and Visible (475–800 nm), respectively, depicting a lifetime enhancement seen for the previously analyzed spot. UFTS is performed in the visible regime, which shows a decrease in differential absorption, and increased roughness increases the probe scattering, which can be seen in the contour plot in Fig. 8(b) and (c). Both regions, i.e., Gold on Planar Si and Gold on structured Si (formed at 5 cm & 8 cm), show a PIA signal owing to intraband transition within the sp-band. The sole variation is a significant shift in the lifetime of relaxing carriers due to the structuring. A positive PIA signal between 500 and 1500 nm is caused by an inter-band transition of gold carriers, which decay significantly more slowly in structured gold films (LIPSS) depicted in Tables 2 and 3.

For visible probe regimes, the planar gold film with three-time constants (τ_1), which is the fastest lifetime observed due to the thermal relaxation of carriers within the sp-band and is of the order of a few hundreds of fs which is also enhanced dramatically more considerable of the order of a few ps. After that, a time constant (τ_2) of an order of few ps is the phonon-phonon scattering and also the transfer of charge to the metal-semiconductor interface and τ_3 which is the slowest time constant, is due to the decay of carriers trapped through surface and tail states of the metal-semiconductor interface is shown in Table 3. Similar behavior was observed in the NIR range (800–1500 nm) with 2-exponential kinetic fit where the corresponding time constants (τ_1) and (τ_2) are the electron-phonon within the band and phonon-phonon

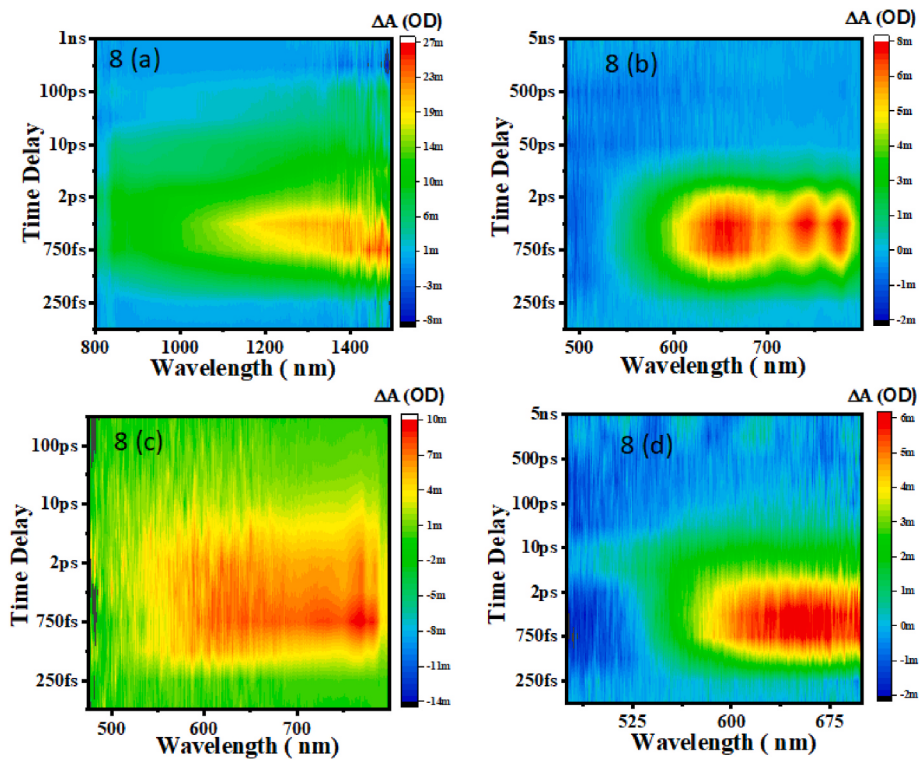


Fig. 8. 2-D color contour plot of transient absorption spectra (a) structure Si (LIPSS at 8 cm) at different NIR probe wavelengths, (b) Gold coated Si at the different visible probe, (c) Gold coated Structured Si (LIPSS at 8 cm) at the different visible probe and (d) Gold coated Structured Si (LIPSS at 5 cm) at the different visible probe.

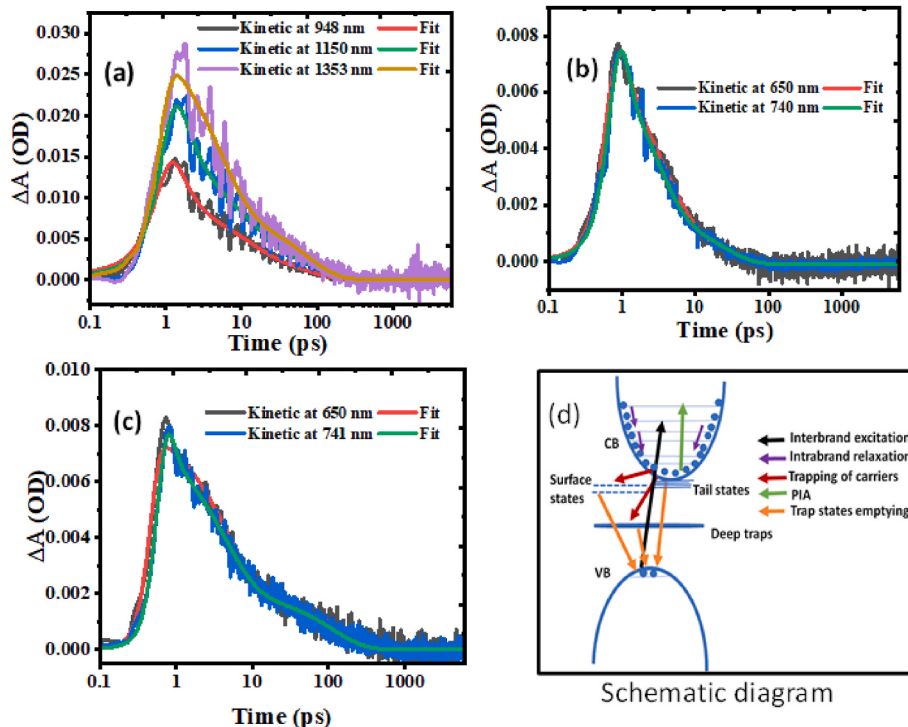


Fig. 9. Kinetic/decay profile, where the X-axis is in log scale, (a) structure Si (LIPSS at 8 cm) at different NIR probe wavelengths, (b) Gold coated Si at the different visible probe, (c) Gold coated Structured Si (LIPSS at 8 cm) at the different visible probe and (d) Schematic diagram for path followed during hot carrier relaxation.

Table 3

Decay Kinetics at different probe wavelengths (Visible) for Gold on plane and gold on structured Si.

Wavelength (nm)	Gold on Si (ps)	Gold on LIPSS (8 cm) (ps)	Gold on LIPSS (5 cm) (ps)
650	$\tau_1 = 0.37$ (43%)	$\tau_1 = 4.67$ (74%)	$\tau_1 = 3.98$ (70%)
	$\tau_2 = 3.35$ (42%)	$\tau_2 = 144$ (26%)	$\tau_2 = 81.9$ (30%)
	$\tau_3 = 21.4$ (15%)		
750	$\tau_1 = 0.87$ (87%)	$\tau_1 = 3.81$ (73%)	–
	$\tau_2 = 2.6$ (9%)	$\tau_2 = 103$ (27%)	–
	$\tau_3 = 23.5$ (4%)		

scattering relaxation to interband respectively as shown in Table 2.

4. Conclusion

This work not only indicated significantly larger lifetime enhancement but also revealed the ultrafast laser-ablation mechanism, nano-ripples formation mechanism, and charge transfer dynamics. The investigation of time-resolved non-equilibrium carrier's dynamics reveals the different pathways for decaying carriers through carrier-carrier relaxation in intraband states, trapping of carriers in defect states, and direct carrier recombination. Interaction of light and material nano-structuring significantly enhances the carrier lifetime owes to carrier confinement in trap-assisted states which restricts the carrier recombination. This nanoscale structuring differs from bulk and can have more exciting carrier transport and optical properties, which helps in improving performance in optoelectronic and nanophotonic devices.

Authors-credit

Kapil kumar: Conceptualisation, Methodology, Investigation, Writing an original draft, Validation, formal analysis, data curation. **Nikita Vashistha:** Helped in LIPSS formation (Experimental work), Image analysis using Software SPIP. **Shivam Tiwari:** Helps in LIPSS formation. **J. S. Tawale:** Performed FE-SEM. **Prince Sharma:** Investigation, formal analysis, data curation, resources. **Mahesh Kumar:** Supervision, project administration, resources, writing (Review and editing), Visualization.

Declaration of competing interest

The authors declare that they have no known competing financial interests or personal relationships that could have appeared to influence the work reported in this paper.

Data availability

The data that supports the findings of this study are available within the article and in supplementary information.

Acknowledgment

The authors would like to thank Director CSIR-NPL for providing the required support. One of the authors, Kapil Kumar, would like to thank Co-Supervisor Prof. Venu Gopal Achanta for constant support and encouragement. He would like to thank UGC for providing the research opportunity and AcSIR for their acceptance as research scholars at CSIR-NPL.

Appendix A. Supplementary data

Supplementary data to this article can be found online at <https://doi.org/10.1016/j.physb.2023.414814>.

References

- [1] A.V. Dostovalov, T.J.Y. Derrien, S.A. Lizunov, F. Preucl, K.A. Okotrub, T. Mocek, V. P. Korolkov, S.A. Babin, N.M. Bulgakova, LIPSS on thin metallic films: New insights from multiplicity of laser-excited electromagnetic modes and efficiency of metal oxidation, *Appl. Surf. Sci.* 491 (2019) 650–658, <https://doi.org/10.1016/j.apsusc.2019.05.171>.
- [2] H.Y. Tsai, S.W. Luo, C.W. Wu, S.H. Wang, Sub-micron-structure machining on silicon by femtosecond laser, *Trans. Nonferrous Metals Soc. China* 19 (1) (2009) 171–177, [https://doi.org/10.1016/S1003-6326\(10\)60266-X](https://doi.org/10.1016/S1003-6326(10)60266-X).
- [3] C. Albu, A. Dinescu, M. Filipescu, M. Ulmeanu, M. Zamfirescu, Periodical structures induced by femtosecond laser on metals in air and liquid environments, *Appl. Surf. Sci.* 278 (2013) 347–351, <https://doi.org/10.1016/j.apsusc.2012.11.075>.
- [4] C.Y. Yu, Y.F. Gao, B. Han, M. Ehrhardt, P. Lorenz, L.F. Xu, R.H. Zhu, Picosecond laser induced periodic surface structures on K9 glass, *Surface. Interfac.* 23 (2021), 101026, <https://doi.org/10.1016/j.surfin.2021.101026>.
- [5] Q. Wu, Y. Ma, R. Fang, Y. Liao, Q. Yu, X. Chen, K. Wang, Femtosecond laser-induced periodic surface structure on diamond film, *Appl. Phys. Lett.* 82 (2003) 1703–1705, <https://doi.org/10.1063/1.1561581>.
- [6] J. Bonse, S. Gräf, Maxwell meets marangoni—a review of theories on laser-induced periodic surface structures, *Laser Photon. Rev.* 14 (10) (2020), 2000215, <https://doi.org/10.1002/lpor.202000215>.
- [7] J. Bonse, S. Hohm, S.V. Kirner, A. Rosenfeld, J. Krüger, Laser-induced periodic surface structures-A scientific evergreen, *IEEE J. Sel. Top. Quant. Electron.* 23 (2017) 109–123, <https://doi.org/10.1109/JSTQE.2016.2614183>.
- [8] S. He, J.J. Nivas, K.K. Anoop, A. Vecchione, M. Hu, R. Bruzzese, S. Amoruso, Surface structures induced by ultrashort laser pulses: formation mechanisms of ripples and grooves, *Appl. Surf. Sci.* 353 (2015) 1214–1222, <https://doi.org/10.1016/j.apsusc.2015.07.016>.
- [9] G. Racuikaitis, Ultra-short pulse lasers for microfabrication: a review, *IEEE J. Sel. Top. Quant. Electron.* 27 (2021) 1–12, <https://doi.org/10.1109/JSTQE.2021.3097009>.
- [10] E.L. Gurevich, Mechanisms of femtosecond LIPSS formation induced by periodic surface temperature modulation, *Appl. Surf. Sci.* 374 (2016) 56–60, <https://doi.org/10.1016/j.apsusc.2015.09.091>.
- [11] F. Pigeon, J.P. Colombier, M. Bounhalli, F. Garrelie, S. Tonchev, S. Reynaud, O. Parriaux, N. Faure, Evidence of surface plasmon resonance in ultrafast laser-induced ripples, *Opt Express* 19 (10) (2011) 9035–9043, <https://doi.org/10.1364/OE.19.009035>.
- [12] E. Devaux, T.W. Ebbesen, J.C. Weeber, A. Dereux, Launching and decoupling surface plasmons via micro-gratings, *Appl. Phys. Lett.* 83 (2003) 4936, <https://doi.org/10.1063/1.1634379>.
- [13] H. Raether, G. Hohler, E.A. Nieirsch, *Surface Plasmons on Smooth and Rough Surfaces and on Gratings*, vol. 111, Springer Tracts in Modern Physics, 1988, p. 136, <https://doi.org/10.1007/BF0048317-COVER>.
- [14] E.L. Gurevich, Mechanisms of femtosecond LIPSS formation induced by periodic surface temperature modulation, *Appl. Surf. Sci.* 374 (2016) 56–60, <https://doi.org/10.1016/J.APSUSC.2015.09.091>.
- [15] H.M. van Driel, J.E. Sipe, J.F. Young, Laser-Induced Periodic Surface Structure on Solids: A Universal Phenomenon, *Phys. Rev. Lett.* 49 (26) (1982) 1955, <https://doi.org/10.1103/PhysRevLett.49.1955>.
- [16] J. Bonse, A. Rosenfeld, J. Krüger, Implications of transient changes of optical and surface properties of solids during femtosecond laser pulse irradiation to the formation of laser-induced periodic surface structures, *Appl. Surf. Sci.* 257 (12) (2011) 5420–5423, <https://doi.org/10.1016/j.apsusc.2010.11.059>.
- [17] S. Bashir, M.S. Rafique, C.S. Nathala, A.A. Ajami, W. Husinsky, Femtosecond laser fluence based nanostructuring of W and Mo in ethanol, *Phys. B Condens. Matter* 513 (2017) 48–57, <https://doi.org/10.1016/j.physb.2017.03.008>.
- [18] O. Varlamova, M. Bounhalli, J. Reif, Influence of irradiation dose on laser-induced surface nanostructures on silicon, *Appl. Surf. Sci.* 278 (2013) 62–66, <https://doi.org/10.1016/j.apsusc.2012.10.140>.
- [19] J. Cui, A. Nogales, T.A. Ezquerra, E. Rebollar, Influence of substrate and film thickness on polymer LIPSS formation, *Appl. Surf. Sci.* 394 (2017) 125–131, <https://doi.org/10.1016/j.apsusc.2016.10.045>.
- [20] S. Schwarz, S. Rung, R. Hellmann, One-dimensional low spatial frequency LIPSS with rotating orientation on fused silica, *Appl. Surf. Sci.* 411 (2017) 113–116, <https://doi.org/10.1016/j.apsusc.2017.02.235>.
- [21] S. Gräf, F.A. Müller, Polarisation-dependent generation of fs-laser induced periodic surface structures, *Appl. Surf. Sci.* 331 (2015) 150–155, <https://doi.org/10.1016/j.apsusc.2015.01.056>.
- [22] S. Maragkaki, T.J.Y. Derrien, Y. Levy, N.M. Bulgakova, A. Ostendorf, E.L. Gurevich, Wavelength dependence of picosecond laser-induced periodic surface structures on copper, *Appl. Surf. Sci.* 417 (2017) 88–92, <https://doi.org/10.1016/j.apsusc.2017.02.068>.
- [23] Y. Fuentes-Edfufi, J.A. Sánchez-Gil, M. García-Pardo, R. Serna, G.D. Tsibidis, V. Giannini, J. Solis, J. Siegel, Tuning the period of femtosecond laser induced surface structures in steel: from angled incidence to quill writing, *Appl. Surf. Sci.* 493 (2019) 948–955, <https://doi.org/10.1016/j.apsusc.2019.07.106>.

- [24] A. Karlash, A. Dmytryuk, I. Dmitruk, N. Berezovska, Y. Hrabovskyi, I. Blonskyi, Impact of wavelength, intensity and polarization on the morphology of femtosecond laser-induced structures on crystalline silicon surface, *Appl. Nanosci.* 12 (2022) 1191–1199, <https://doi.org/10.1007/s13204-021-01823-6>.
- [25] Y. Du, M. Zhu, Z. Sui, K. Yi, Y. Jin, H. He, Antireflective sub-wavelength structures on fused silica via self-assembly of silica, *Thin Solid Films* 548 (2013) 103–108, <https://doi.org/10.1016/j.tsf.2013.09.004>.
- [26] A. San-Blas, M. Martinez-Calderon, J. Buencuerpo, L.M. Sanchez-Brea, J. del Hoyo, M. Gómez-Aranzadi, A. Rodríguez, S.M. Olaizola, Femtosecond laser fabrication of LIPSS-based waveplates on metallic surfaces, *Appl. Surf. Sci.* 520 (2020), 146328, <https://doi.org/10.1016/JAPSUSC.2020.146328>.
- [27] A.Y. Vorobyev, C. Guo, Colorizing metals with femtosecond laser pulses, *Appl. Phys. Lett.* 92 (2008), 041914, <https://doi.org/10.1063/1.2834902>.
- [28] J. Chen, Z. Liu, F. Su, S. Wu, C. Liang, J. Liu, Surface modification of carbon fiber cloth by femtosecond laser direct writing technology, *Mater. Lett.* 323 (2022), 132483, <https://doi.org/10.1016/J.MATLET.2022.132483>.
- [29] N. Božinović, V. Rajić, D. Kisić, D. Milovanović, J. Savović, S. Petrović, Laser surface texturing of Ti/Cu/Ti and Ti/Cu/Zr/Ti multilayers thin films, *Opt. Quant. Electron.* 54 (2022) 1–12, <https://doi.org/10.1007/S11082-022-03910-6>.
- [30] J.S. Hwang, J.E. Park, G.W. Kim, H. Lee, M. Yang, Fabrication of printable nanograting using solution-based laser-induced periodic surface structure process, *Appl. Surf. Sci.* 547 (2021), 149178, <https://doi.org/10.1016/JAPSUSC.2021.149178>.
- [31] P. Nürnberg, H.M. Reinhardt, D. Rhinow, R. Riedel, S. Werner, N.A. Hampp, Controlled growth of periodically aligned copper-silicide nanocrystal arrays on silicon directed by laser-induced periodic surface structures (LIPSS), *Appl. Surf. Sci.* 420 (2017) 70–76, <https://doi.org/10.1016/JAPSUSC.2017.05.005>.
- [32] N. Asgari, S.M. Hamidi, Exciton-plasmon coupling in two-dimensional plexitonic nano grating, *Opt. Mater.* 81 (2018) 45–54, <https://doi.org/10.1016/j.optmat.2018.05.011>.
- [33] J.G.A.B. Simões, R. Riva, W. Miyakawa, High-speed Laser-Induced Periodic Surface Structures (LIPSS) generation on stainless steel surface using a nanosecond pulsed laser, *Surf. Coat. Technol.* 344 (2018) 423–432, <https://doi.org/10.1016/j.surfcoat.2018.03.052>.
- [34] L. Yang, A. El-Tamer, U. Hinze, J. Li, Y. Hu, W. Huang, J. Chu, B.N. Chichkov, Parallel direct laser writing of micro-optical and photonic structures using spatial light modulator, *Opt. Laser Eng.* 70 (2015) 26–32, <https://doi.org/10.1016/j.optlaseng.2015.02.006>.
- [35] Z.L. Wu, Y.N. Qi, X.J. Yin, X. Yang, C.M. Chen, J.Y. Yu, J.C. Yu, Y.M. Lin, F. Hui, P. L. Liu, Y.X. Liang, Y. Zhang, M.S. Zhao, Polymer-based device fabrication and applications using direct laser writing technology, *Polymers* 11 (2019) 553, <https://doi.org/10.3390/polym11030553>.
- [36] Q. Huang, X. Zhan, Z. Hou, Q. Chen, H. Xu, Polymer photonic-molecule microlaser fabricated by femtosecond laser direct writing, *Opt. Commun.* 362 (2016) 73–76, <https://doi.org/10.1016/j.optcom.2015.08.018>.
- [37] A.S. Alnaser, S.A. Khan, R.A. Ganeev, E. Stratakis, Recent advances in femtosecond laser-induced surface structuring for oil-water separation, *Appl. Sci.* 9 (8) (2019) 1554, <https://doi.org/10.3390/app9081554>.
- [38] C. Kunz, J. Bonse, D. Spaltmann, C. Neumann, A. Turchanin, J.F. Bartolomé, F. A. Müller, S. Gräf, Tribological performance of metal-reinforced ceramic composites selectively structured with femtosecond laser-induced periodic surface structures, *Appl. Surf. Sci.* 499 (2020), 143917, <https://doi.org/10.1016/j.apsusc.2019.143917>.
- [39] S. Hamad, S.S. Bharati Moram, B. Yendeti, G.K. Podagatlappali, S.V.S. Nageswara Rao, A.P. Pathak, M.A. Mohiddon, V.R. Soma, Femtosecond laser-induced, nanoparticle-embedded periodic surface structures on crystalline silicon for reproducible and multi-utility SERS platforms, *ACS Omega* 3 (2018) 18420–18432, <https://doi.org/10.1021/acsomega.8b02629>.
- [40] A. di Cicco, G. Polzoni, R. Gunnella, A. Trapananti, M. Minicucci, S.J. Rezvani, D. Catone, L. di Mario, J.S. Pelli Cresi, S. Turchini, F. Martelli, Broadband optical ultrafast reflectivity of Si, Ge and GaAs, *Sci. Rep.* 10 (2020), 17363, <https://doi.org/10.1038/s41598-020-74068-y>.
- [41] A.J. Sabbah, D.M. Riffe, Femtosecond pump-probe reflectivity study of silicon carrier dynamics, *Phys. Rev. B Condens. Matter* 66 (2002) 1–11, <https://doi.org/10.1103/PhysRevB.66.165217>.
- [42] E. Lioudakis, A. Othonos, A.G. Nassiopoulou, Ultrafast transient photoinduced absorption in silicon nanocrystals: coupling of oxygen-related states to quantized sublevels, *Appl. Phys. Lett.* 90 (2007), 171103, <https://doi.org/10.1063/1.2728756>.
- [43] R. Gunnella, G. Zgrablic, E. Giangrisostomi, F. D'Amico, E. Principi, C. Masciovecchio, A. di Cicco, F. Parmigiani, Ultrafast reflectivity dynamics of highly excited Si surfaces below the melting transition, *Phys. Rev. B* 94 (15) (2016), 155427, <https://doi.org/10.1103/PhysRevB.94.155427>.
- [44] A. Esser, W. Kütt, M. Strähnen, G. Maidorn, H. Kurz, Femtosecond transient reflectivity measurements as a probe for process-induced defects in silicon, *Appl. Surf. Sci.* 46 (1990) 446–450, [https://doi.org/10.1016/0169-4332\(90\)90187-5](https://doi.org/10.1016/0169-4332(90)90187-5).
- [45] A.J. Sabbah, D.M. Riffe, Measurement of silicon surface recombination velocity using ultrafast pump-probe reflectivity in the near infrared, *J. Appl. Phys.* 88 (2000) 6954–6956, <https://doi.org/10.1063/1.1316047>.
- [46] M.S. Tyagi, R. van Overstraeten, Minority carrier recombination in heavily-doped silicon, *Solid-State Electron.* 26 (6) (1983) 577–597, [https://doi.org/10.1016/0038-1101\(83\)90174-0](https://doi.org/10.1016/0038-1101(83)90174-0).
- [47] A. Cuevas, D. Macdonald, Measuring and interpreting the lifetime of silicon wafers, *Sol. Energy* 76 (2004) 255–262, <https://doi.org/10.1016/j.solener.2003.07.033>.
- [48] D. Cavalcoli, B. Fraboni, A. Cavallini, Surface and defect states in semiconductors investigated by surface photovoltaic, in: *Semiconductors and Semimetals*, vol. 91, Academic Press Inc., 2015, pp. 251–278, <https://doi.org/10.1016/bs.semsem.2014.11.004>.
- [49] L. Burstein, Y. Shapira, J. Partee, J. Shinar, Y. Lubianiker, I. Balberg, Surface photovoltaic spectroscopy of porous silicon, *Phys. Rev. B* 55.4 (1997) R1930, <https://doi.org/10.1103/PhysRevB.55.R1930>.
- [50] J.F. Wager, Real- and reciprocal-space attributes of band tail states, *AIP Adv.* 7 (2017), 125321, <https://doi.org/10.1063/1.5008521>.
- [51] N.A. Modine, A.M. Armstrong, M.H. Crawford, W.W. Chow, Highly nonlinear defect-induced carrier recombination rates in semiconductors, *J. Appl. Phys.* 114 (2013), 144502, <https://doi.org/10.1063/1.4824065>.
- [52] M.K. Hsieh, K.N. Ku, M.C.M. Lee, Enhanced photon-induced carrier density in silicon-on-insulator via surface recombination suppression for increasing plasma dispersion effect, *J. Appl. Phys.* 105 (7) (2009), 074510, <https://doi.org/10.1063/1.3106527>.
- [53] Y. Ma, H. Ren, J. Si, X. Sun, H. Shi, T. Chen, F. Chen, X. Hou, An alternative approach for femtosecond laser induced black silicon in ambient air, *Appl. Surf. Sci.* 261 (2012) 722–726, <https://doi.org/10.1016/j.apsusc.2012.08.087>.
- [54] J. Huang, K. Xu, J. Hu, D. Yuan, J. Li, J. Qiao, S. Xu, Self-Aligned plasmonic lithography for maskless fabrication of large-area long-range ordered 2D nanostructures, *Nano Lett.* 54 (2022) 20, <https://doi.org/10.1021/ACS.NANOlett.2C01740>.
- [55] J.S. Villarrubia, Algorithms for scanned probe microscope image simulation, surface reconstruction, and tip estimation, *J. Res. Natl. Inst. Stand. Technol.* 102 (1997) 425–454, <https://doi.org/10.6028/JRES.102.030>.
- [56] J.F. Jorgensen, K. Carneiro, L.L. Madsen, The scanning tunneling microscope and surface characterization, *Nanotechnology* 4 (1993) 152, <https://doi.org/10.1088/0957-4484/4/3/004>.
- [57] N. Vashistha, A. Kumar, R.K. Singh, M. Kumar, Wavelength and decay time tuning of intraband transitions in low spatial frequency laser-induced periodic surface structures, *Optik* 246 (2021), 167833, <https://doi.org/10.1016/J.IJLEO.2021.167833>.
- [58] S.K. Saini, P. Sharma, N. Vashistha, L. Tyagi, M. Kumar, Structural correlation of phonon dynamics in Bismuth and Tellurium for the formation of Bismuth Telluride, using ultrafast transient absorption spectroscopy, *Phys. B Condens. Matter* 638 (2022), 413935, <https://doi.org/10.1016/J.PHYSB.2022.413935>.
- [59] T. Apostolova, B. Obreshkov, I. Gnilitsky, Ultrafast energy absorption and photoexcitation of bulk plasmon in crystalline silicon subjected to intense near-infrared ultrashort laser pulses, *Appl. Surf. Sci.* 519 (2020), 146087, <https://doi.org/10.1016/JAPSUSC.2020.146087>.
- [60] E. Lioudakis, A. Othonos, A.G. Nassiopoulou, Ultrafast transient photoinduced absorption in silicon nanocrystals: coupling of oxygen-related states to quantized sublevels, *Appl. Phys. Lett.* 90 (2007), 171103, <https://doi.org/10.1063/1.2728756>.
- [61] S.K. Saini, N. Kumar Tailor, P. Sharma, L. Tyagi, N. Vashistha, R. Yadav, A. Kumar Chaudhary, S. Satapathi, M. Kumar, S.K. Saini, P. Sharma, N. Vashistha, R. Yadav, A.K. Chaudhary, M. Kumar, N.K. Tailor, S. Satapathi, L. Tyagi, Revealing the substrate dependent ultrafast phonon dynamics in Bi₂Se₃ thin films, *Adv. Mater. Interfac.* (2022), 2201650, <https://doi.org/10.1002/ADMI.202201650>.
- [62] M. Otto, M. Kroll, T. Käsebier, R. Salzer, A. Tünnermann, R.B. Wehrspohn, Extremely low surface recombination velocities in black silicon passivated by atomic layer deposition, *Appl. Phys. Lett.* 100 (2012), 191603, <https://doi.org/10.1063/1.4714546>.